Two-electron atoms in short intense laser pulses

Armin Scrinzi[1] and Bernard Piraux[2]
[1]*Institut für Theoretische Physik, Universität Innsbruck, Technikerstrasse 25, A-6020 Innsbruck, Austria*
[2]*Institut de Physique, Université Catholique de Louvain, 2, Chemin du Cyclotron, B-1348 Louvain-la-Neuve, Belgium*
(Received 27 February 1998)

We discuss a method of solving the time-dependent Schrödinger equation for atoms with two active electrons in a strong laser field, which we used in a previous paper [A. Scrinzi and B. Piraux, Phys. Rev. A **56**, R13 (1997)] to calculate ionization, double excitation, and harmonic generation in helium by short laser pulses. The method employs complex scaling and an expansion in an explicitly correlated basis. Convergence of the calculations is documented and error estimates are provided. The results for He at peak intensities up to 10^{15} W/cm^2 and wavelength 248 nm are accurate to at least 10%. Similarly accurate calculations are presented for electron detachment and double excitation of the negative hydrogen ion. [S1050-2947(98)00208-X]

PACS number(s): 32.80.Rm, 32.80.Fb

I. INTRODUCTION

Several programs are being pursued that aim at a description of three-dimensional two-electron or multielectron atoms in strong laser fields [1–4]. The common motivation for these efforts is to obtain quantitative results for excitation, ionization, and generation of harmonics by laser pulses at intensities, where more than one electron participates in the process. The various approaches emphasize different aspects of the problem.

The first fully correlated three-dimensional calculations for two-electron atoms in nonperturbative laser fields were made for constant laser intensity by the *R*-matrix Floquet method [1]. Results have been published on H^- and He [5] and Mg [6]. The advantage of the method is that it can be applied to multielectron atoms, where existing atomic structure programs can be used. At large intensities, many angular momenta and Floquet blocks are required, and very large systems of equations have to be solved. Recently an adaptation of the *R*-matrix method to solve the time-dependent Schrödinger equation was proposed [2], which maintains the applicability to general atoms, but may be less plagued by expansion size problems.

The approach of Ref. [3] puts a strong emphasis on two-electron correlation in He-like atoms at the expense of abandoning the realistic description of atomic structure. The method solves the time-dependent Schrödinger equation on a grid for the radial electron coordinates, and with an expansion in single-particle spherical harmonics for the angular degrees of freedom. By visualization of the wave function, in particular the process of direct double ionization could be studied. The implementation is adjusted to a massively parallel computer, but still the grid size and the length of the multipole expansion of the interelectron potential is limited by computer resources.

The method of Ref. [4] describes a two-electron wave function by an expansion in numerical single-electron wave functions that are calculated in a finite box. This provides a realistic representation of atomic structure, and allows one to adjust the wave function to the parameter range to be investigated. For example, when photoelectron spectra are to be extracted, continuous wave functions can be densely placed in range of electron energies of interest. Results have been published on Mg [7].

Here we present in detail the method employed for the calculation of excitation, ionization, and harmonic generation in He published in a previous paper [8]. Our purpose is to provide converged *ab initio* calculations for realistic laser parameters, with special emphasis on electron correlation. We use an expansion in explicitly correlated two-electron basis functions and complex scaling [9]. The range of application is similar to that of Ref. [4]. The most important difference is our use of an explicitly correlated basis, which gives a very accurate description of atomic structure including doubly excited states with a relatively short expansion. The second crucial ingredient of our method is complex scaling which, as we will show, gives a simple implementation of strictly outgoing wave boundary conditions by an L^2 method. The penalty of the method is the loss of a direct physical interpretation of the continuous spectrum of the complex scaled operator. While this may not be a fundamental limitation of the complex scaling method, it does at present limit our results to total ionization, double excitation, and harmonic generation.

Compared to Ref. [8], we extend the calculations for He to higher laser intensities up to 10^{15} W/cm^2 at a laser wavelength of 248 nm. The foundation of the error estimates given in Ref. [8] is presented and discussed in detail. By improvements of the basis the accuracy of the harmonic spectra calculation could be enhanced to about 10%. We supplement the results by laser detachment and double excitation of H^-.

II. COMPUTATIONAL METHOD

The Schrödinger equation of a two-electron atom exposed to a laser field described in velocity gauge with the dipole approximation is

$$i\frac{d}{dt}\Psi(\vec{r}_1,\vec{r}_2;t)=\left[H_0+\frac{i}{c}\vec{A}(t)\cdot(\vec{\nabla}_1+\vec{\nabla}_2)\right]\Psi(\vec{r}_1,\vec{r}_2;t), \tag{1}$$

with the atomic Hamiltonian

$$H_0 = -\frac{1}{2}(\Delta_1+\Delta_2) - \frac{Z}{r_1} - \frac{Z}{r_2} + \frac{1}{|\vec{r}_1-\vec{r}_2|}, \qquad (2)$$

where $\vec{r}_1$ and $\vec{r}_2$ denote the electron coordinates measured from the nucleus, and Δ_i and $\vec{\nabla}_i$ are the corresponding Laplace and gradient operators. The nuclear charge is $Z=2$ for He and $Z=1$ for the negative hydrogen ion. Atomic units are used unless stated otherwise.

The vector potential of a linearly polarized laser pulse is given by

$$\vec{A}(t) = h(t)\sin(\omega t)(0,0,A_0), \qquad (3)$$

where we employed $\cos^2$ and Gaussian shaped envelopes

$$h_{\cos^2}(t) = [\cos(\pi t/T)]^2,$$

$$h_{\mathrm{Gauss}}(t) = \exp[-(2t/T)^2],$$

with the pulse duration T.

The calculations were made in velocity gauge, since we found much better convergence than in length gauge, which is in agreement with previous experience and with theoretical arguments [10]. A calculation at intensity 10^{14} W/cm^2 and frequencies of $\omega=0.4$ and 0.6 was repeated in length gauge, and gave the same results for ionization and single excitation. Results for double excitation could not be converged in length gauge.

Equation (1) is a $(6+1)$-dimensional equation, which can be reduced to $5+1$ dimensions because of cylindrical symmetry, when the laser is linearly polarized. Due to the high dimensionality only a very limited range of the phase space can be numerically represented, and one needs to control the restrictions imposed on this space carefully. The restrictions consist of basis set truncation and the boundary conditions at large distance. We first discuss the boundary conditions.

A. Absorption of outgoing flux

Ionization means that a finite portion of the wave function moves away to arbitrarily large distances without further contributing to the dynamics of the system. In a finite space, one needs to absorb this outgoing flux at the boundary of the space to avoid unphysical reflections. Common procedures are the use of a complex potential at large distances [11,2], or some form of mask function [3]. A more systematic control of the asymptotic boundary conditions was proposed in Ref. [12]. Ideally, one admits only outgoing waves at large distances. However, outgoing-wave boundary conditions are difficult to define in the presence of a dipole field, which ranges to arbitrarily large distances. In any case, correctly imposed outgoing-wave boundary conditions are energy dependent, which is, in general, quite difficult to implement computationally. An additional complication is that the resulting Hamiltonian is non-self-adjoint (the norm of the wave function on the finite space is not conserved) and it has nonorthogonal eigenfunctions. This may cause problems for computational implementations that rely on the orthogonality of the eigenfunctions of the Hamiltonian.

For calculations with only one active electron, which are effectively $2+1$ dimensional, one can usually make the space large enough such that the boundary conditions are of secondary importance. In our case, a more stringent method of absorbing outgoing flux is required. Such a method is complex scaling [9,13]. It consists in analytically continuing the Hamiltonian by multiplying the real coordinates by a complex number

$$H(\vec{r}_1,\vec{r}_2;t) \rightarrow H_\theta = H(e^{i\theta}\vec{r}_1, e^{i\theta}\vec{r}_2;t), \qquad (4)$$

where the scaling angle θ is real and positive. For the time-independent Schrödinger equation, the mathematical theory of complex scaling is well established. The new Hamiltonian H_θ has the same bound-state spectrum as H, while the continuous spectrum is rotated by the angle -2θ around the ionization thresholds into the lower half-plane of complex energies. This separates the continua starting from different ionization thresholds. In the wedge-shaped area between the real axis and the rotated continua, doubly excited states appear as square-integrable eigenfunctions with complex eigenvalues, whose imaginary parts give one-half of the autoionization widths. In an exact calculation, the values of bound-state and resonance energies do not depend on the scaling angle θ. The method is being widely applied. For multiphoton physics it is used to calculate ionization rates and ac Stark shifts of hydrogenlike systems by the Floquet method, and in time-dependent calculations for hydrogenlike systems [14,15].

There is no complete mathematical theory for the application of complex scaling to time-dependent problems; only partial results for the time evolution of bound and resonance states were found [16]. In the Appendix we argue that the restriction of the complex scaled Schrödinger equation

$$i\frac{d}{dt}\Psi_\theta(\vec{r}_1,\vec{r}_2;t) = H_\theta\Psi_\theta(\vec{r}_1,\vec{r}_2;t) \qquad (5)$$

to the space of square-integrable functions is equivalent to an unscaled equation with the constraint of strictly outgoing-wave boundary conditions. The outgoing-wave solution at the coordinates $(\vec{r}_1,\vec{r}_2)$ is obtained by evaluating Ψ_θ at the back-scaled arguments $(e^{-i\theta}\vec{r}_1, e^{-i\theta}\vec{r}_2)$. To establish this equivalence, we need to assume far reaching analyticity properties of the solution $\Psi_\theta(\vec{r}_1,\vec{r}_2;t)$, which are difficult to prove in practice.

Regardless of this mathematical problem, the method has been successfully employed in time-dependent calculations [15], and its validity could be verified numerically [17]. For hydrogen one can approach the limit $\theta\rightarrow 0$, i.e., directly compare with the usual Schrödinger equation. It was found that the projections on bound states and the expectation value of the dipole

$$\vec{d}(t) = -\langle\Psi_\theta(e^{-i\theta}\vec{r},t)|\vec{r}|\Psi_\theta(e^{-i\theta}\vec{r},t)\rangle \qquad (6)$$

do not depend on the scaling angle θ. The advantage of the complex scaled solution is that, due to the absence of reflections, a much shorter expansion of the wave function can be used when $\theta\neq 0$. For the two-electron system, basis size requirements exclude very small scaling angles, but we found stable results for the excited state populations and for $\vec{d}(t)$ in the range of $0.12\lesssim\theta\lesssim 0.28$ (see below).

The harmonic spectrum is obtained by Fourier transforming the acceleration of the dipole $\ddot{\vec{d}}$. The total ionization yield is defined as

$$Y_{\text{ion}}=1-\sum_i |\langle\Phi_i(\vec{r}_1,\vec{r}_2)|\Psi_\theta(e^{-i\theta}\vec{r}_1,\vec{r}_2;t=\infty)\rangle|^2, \quad (7)$$

where Φ_i is the ith bound-state function calculated with the real Hamiltonian $H_{\theta=0}$. We use the computationally more convenient formula

$$Y_{\text{ion}}=1-\sum_i |\langle\Phi^*_{i,\theta}(\vec{r}_1,\vec{r}_2)|\Psi_\theta(\vec{r}_1,\vec{r}_2;t=\infty)\rangle|^2, \quad (8)$$

where $\Phi_{i,\theta}$ is the bound-state eigenfunction of the complex scaled atomic Hamiltonian

$$H_{0,\theta}\Phi_{i,\theta}=E_i\Phi_{i,\theta}. \quad (9)$$

Note the extra complex conjugation on the left-hand function, i.e., in the integral the *unconjugated* function is used. Equations (7) and (8) are equivalent because of the analyticity of both $\Phi_{i,\theta}$ and Ψ_θ, and since for $\theta=0$, $\Phi_{i,\theta=0}$ is real up to an overall phase (see the Appendix).

The population of a doubly excited state α is determined as

$$P_\alpha=|\langle\Phi^*_{\alpha,\theta}|\Psi_\theta\rangle|^2. \quad (10)$$

This equation does not have an unscaled analog, since the resonance wave function $\Phi_{\alpha,\theta}$ seizes to be square integrable when θ approaches 0.

B. Basis set expansion

We approximate the solution of the complex scaled Schrödinger equation by expanding Ψ_θ in a Hylleraas-like explicitly correlated basis

$$\Psi_\theta(\vec{r}_1,\vec{r}_2;t) = P_1\sum_{L=0}^{L_{\max}}\sum_{l=0}^{L} G_{Ll}(\vec{r}_1,\vec{r}_2) \times\sum_s\sum_{k=0}^{k_s}\sum_{m=0}^{m_s}\sum_{n=0}^{n_s} c^{Ll}_{kmn;s}(t)r_1^k r_2^m r_{12}^n e^{-\alpha_s r_1-\beta_s r_2} \quad (11)$$

The operator P_1 projects on the singlet states, and $r_{12}:=|\vec{r}_1-\vec{r}_2|$. The two-electron angular factors G_{Ll} for total angular momentum L and z component $L_z=0$ are

$$G_{Ll}=r_1^l r_2^{L-l}\sum_m C^{L,0}_{l,m;L-l,-m}Y^l_m(\hat{r}_1)Y^{L-l}_{-m}(\hat{r}_2). \quad (12)$$

$C^{L,0}_{l,m;L-l,-m}$ are Clebsch-Gordan coefficients, and Y^l_m are spherical harmonics. Note that for each L there are only $L+1$ angular functions $G_{L,l}$. The major part of the angular correlation, which in the usual atomic physics basis requires a large number of combinations of single-electron angular momenta l and $L-l$, is here contained in the interelectron coordinate r_{12}.

TABLE I. Basis set for $L=2$ used in time propagation. ''Size'' denotes the number of basis functions. For the time propagation, near linearly dependent vectors are removed.

l	α_s	β_s	k_s	m_s	n_s	p_s	Size
0	−2.000	−0.333	3	9	2	9	
	−2.000	−0.250	3	9	2	9	
	−2.000	−0.200	4	9	2	9	221
1	−1.400	−1.400	6	6	2	6	
	−0.666	−0.666	6	6	2	6	56
2	−2.900	−2.900	1	1	1	1	
	−1.400	−1.400	6	6	2	6	
	−1.000	−1.000	6	6	2	6	
	−0.666	−0.666	6	6	2	6	139
total							416
total in time propagation							318

Expansion (11) is known to be formally complete [18], and it converges rapidly for bound states of the three-body Coulomb system. In Ref. [19], a further significant improvement of the basis was achieved by selecting the combination of powers by the rule

$$k+m+n+|k-m|(1-\delta_{0n})\leqslant p_s. \quad (13)$$

This constraint can be understood as follows: The range of space covered by a basis function in the direction of r_1 and r_2 is roughly k/α_s and m/β_s, respectively. When $\alpha_s\sim\beta_s$, and $|k-m|$ becomes large, the electrons remain far from each other and correlation, which is mostly contained in the coordinate r_{12}, becomes small. One therefore needs fewer functions with r_{12} dependence when $|k-m|$ is large. The constraint leads to an important reduction in the expansion size without deteriorating the accuracy of bound and doubly excited state energies.

In Refs. [19,20] for each state of helium, two sets of exponents were used, one describing the known asymptotic behavior of the bound-state wave function by selecting $\alpha_1=Z$ and $\beta_1=\sqrt{-Z^2-2E}$, and a second one describing correlation by exponents $\alpha_2=\beta_2$, which were optimized to obtain the best bound-state energy E. In our case we needed to describe many states, including strongly correlated doubly excited states, within the same basis set. Therefore we used several different sets of exponents for each L and l. As an example, the exponents and the powers used for $L=2$ in the major part of the calculations are given in Table I. The first group of exponents is adjusted to describe the singly excited states and single-electron continuum of the configuration type $(1s,n'd)$, the middle group is for symmetrically doubly excited states and higher continua of the form $(np,n'p)$ and the last group is for states $(nd,n's)$ with single-electron quantum numbers $n,n'=1,2,3$. The particle-exchanged configurations are automatically included by the exchange symmetrization of the basis functions.

It is important to observe that in velocity gauge double excitation must be included into the basis for a correct rep-

resentation of the wave function, even when no real double excitation occurs. The reason is that the gauge transformation

$$\Psi(\vec{r}_1,\vec{r}_2;t)\rightarrow e^{i\vec{A}(t)\cdot(\vec{r}_1+\vec{r}_2)}\Psi(\vec{r}_1,\vec{r}_2;t) \tag{14}$$

equally affects both coordinates, and thus introduces virtual double excitation.

Our basis functions $G_{Ll}(\vec{r}_1,\vec{r}_2)r_1^k r_2^m r_{12}^n e^{-\alpha_s r_1-\beta_s r_2}$ are strictly real, such that the phase as well as the θ dependence of $\Psi_\theta(\vec{r}_1,\vec{r}_2;t)$ is entirely contained in the expansion coefficients. This means that the expansion coefficients of our complex scaled initial state $\Phi_{\theta,1S}(\vec{r}_1,\vec{r}_2)$ are dependent on θ and for each θ, and a different system of equations with different initial condition has to be solved.

We can interpret the same fact in terms of the back-scaled solution $\Psi_\theta(e^{-i\theta}\vec{r}_1,e^{-i\theta}\vec{r}_2;t)$, which approximates the solution of the normal Schrödinger equation with outgoing-wave boundary conditions. The expansion functions for the outgoing-wave solution are then

$$e^{-i(L+k+m+n)\theta}G_{Ll}(\vec{r}_1,\vec{r}_2)r_1^k r_2^m r_{12}^n e^{-e^{-i\theta}(\alpha_s r_1+\beta_s r_2)},$$

i.e., they strongly depend on θ. By varying θ we therefore vary the expansion functions for the physical solution, and in this way we obtain an estimate of the basis set truncation error with respect to the radial coordinates r_1, r_2, and r_{12}.

C. Alternative basis sets

The good performance of expansion (11) for He is due to the fact that, on the one hand, it is very similar to the usual atomic physics expansion in terms of products of single-electron orbitals, which converges well for states, where the two electrons remain spatially separated. On the other hand, the explicit dependence on r_{12} allows a good description of the wave function at small interelectronic distances, which is particularly important when both electrons are in the same shell, as in the ground state or in symmetrically excited states. We investigated several other expansions, which seem offer technical advantages or which are particularly suitable for specific states of He.

An implementation of arbitrary angular momentum for few-body systems is given by Wigner's D functions [21,22]. At high angular momenta, that expansion allows a strong reduction of the number of nonzero matrix elements in the calculation [23]. The D functions separate the overall rotation of the system from internal degrees of freedom. The overall rotation is defined as the rotation between a body-fixed coordinate system, determined by two vectors $\vec{a}$ and $\vec{b}$, and the laboratory coordinates. The D functions carry indices D^L_{mn}, which designate the total angular momentum L, the quantum number m of rotation around the lab-fixed z axis, and the quantum number n of the rotation around $\vec{a}$. Although there is a certain freedom of choice for $\vec{a}$ and $\vec{b}$, they cannot be identified with the electron coordinates $\hat{r}_1$ and $\hat{r}_2$, since the definition of the D functions is not symmetric under exchange of $\vec{a}$ and $\vec{b}$. In order to implement electron exchange symmetry, one can, for example, use the Jacobi coordinates

$$\vec{a}=\vec{r}_1+\vec{r}_2,$$

$$\vec{b}=\vec{r}_1-\vec{r}_2$$

as the body-fixed vectors. With this choice, the subscripts of D^L_{mn} refer to collective rotations of the electrons. This is desirable for some highly correlated states, like the Wannier states [24]. In the unsymmetrically excited states that dominate the wave function of an atom excited by a laser pulse, one electron carries the major part of angular momentum (except for symmetrization), which leads to poor convergence of the D-function expansion.

Similar problems arise for an expansion with respect to the perimetric coordinates

$$u=-r_1+r_2+r_{12},$$

$$v=r_1-r_2+r_{12},$$

$$w=r_1+r_2-r_{12}.$$

While the interparticle coordinates r_1, r_2, and r_{12} are subject to the triangular inequality $|r_1-r_2|\leqslant r_{12}\leqslant r_1+r_2$, the perimetric coordinates u, v, and w each vary independently in $[0,\infty)$. This simplifies the calculation of integrals, and allows one to find expansion functions, where the operator matrices become sparse. Like with the Jacobi coordinates, the unsymmetrically excited states, where the two electrons move largely independently, are not efficiently described by such an expansion, since u, v, and w each contain both coordinates r_1 and r_2. It also appears difficult to find a constraint like Eq. (13) to cut down on the basis size.

Finally, we explored an expansion with respect to the coordinates r_1, r_2, and $\cos\theta_{12}:=\hat{r}_1\cdot\hat{r}_2$. This is very similar to an expansion in single-electron orbitals. The main advantage is that the calculation of matrix elements becomes simple. However, the expansion length is generally larger than with the explicitly correlated basis, and bound-state accuracies beyond 10^{-4} a.u. become extremely hard to achieve [23].

D. Numerics and computation

Expansion (11) is notoriously numerically difficult. The main reason is that the metrical matrix

$$S_{ij}:=\langle i|j\rangle \tag{15}$$

for the basis functions

$$|i\rangle=G_{Ll}(\vec{r}_1,\vec{r}_2)r_1^{k_i}r_2^{m_i}r_{12}^{n_i}e^{-\alpha_s r_1-\beta_s r_2} \tag{16}$$

rapidly becomes ill conditioned with increasing powers k_i, m_i, and n_i. The situation is further aggravated by our use of several different sets of exponents α_s and β_s for the same L, which makes the basis formally overcomplete. We were able to control these problems by performing accurate integrations, by appropriately normalizing the basis, and by removing near-singular values from the metrical matrix. Still, at high angular momenta we needed to resort to Fortran REAL*16 ($\approx$32 decimal digits) accuracy in the calculation of the matrix elements.

We first express the angular factors in the form

$$G(\vec{r}_1,\vec{r}_2)=\sum_j g_j r_1^{k_j} r_2^{m_j} r_{12}^{n_j} (\cos\theta_1)^{\lambda_j} (\cos\theta_2)^{\mu_j}, \quad (17)$$

where $\cos\theta_i$ is the cosine of $\vec{r}_i$ with the z axis. The determination of the expansion coefficients g_j is straightforward but a little cumbersome. Except for an insignificant overall factor, g_j are rational numbers with not too large denominators, which allowed us to compute them numerically, and to ensure that they were accurate to all digits of arithmetic precision.

For the angular integration we change variables to $\cos\theta_1$, φ_1, $\cos\theta_{12}$, and φ_{12}, where φ_1 is the azimuthal angle of $\vec{r}_1$, $\cos\theta_{12}=\hat{r}_1\cdot\hat{r}_2$, and φ_{12} is the azimuthal angle of $\vec{r}_2$ with respect to the axis $\vec{r}_1$. Integrations can then be performed over all angular variables except for $\cos\theta_{12}$, which is expressed as $\cos\theta_{12}=(r_1^2+r_2^2-r_{12}^2)/(2r_1r_2)$. The remaining three-dimensional integrals have the general form

$$\int dr_1 dr_2 dr_{12} r_1^k r_2^m r_{12}^n e^{-\alpha r_1-\beta r_2}. \quad (18)$$

The integrals are nontrivial, because r_1, r_2, and r_{12} are connected by the triangular inequality. We compute them by a strictly positive and therefore numerically stable recurrence formula [25].

Loss of accuracy is due to the expansions of G_{Ll} and $\cos\theta_{12}$, which at high L become very lengthy with up to several hundred terms. Beyond $L\approx 5$ we needed to use Fortran REAL*16 arithmetic, which provided stable results up to $L\approx 12$.

Even when no accuracy is lost in the matrix elements, the metrical matrix S has in general a very poor condition number which quickly exceeds regular machine precision (≈ 14 decimal digits) or even REAL*16 precision (≈ 32 decimal digits). This may lead to uncontrolled errors. We remove the problem by first rescaling the basis such that the diagonal elements of the metrical matrix are $S_{ii}\equiv 1$, after which the maximum size of the eigenvalues of S was limited to $\lesssim 100$. We diagonalize S and remove eigenvectors with eigenvalues smaller than a threshold ϵ. We found $\epsilon=10^{-11}$ to be suitable for Fortran REAL*8 arithmetic. In REAL*16, we could use $\epsilon=10^{-30}$, but results were found to depend very weakly on the threshold. The remaining eigenvectors $|\xi_i\rangle$ are normalized with respect to S:

$$\langle\xi_i|S|\xi_j\rangle=\delta_{ij}. \quad (19)$$

After transforming all matrices to the orthonormal basis $\{|\xi_i\rangle\}$, precision can be lowered to REAL*8 to save on storage and computation time.

E. Time propagation

For the time propagation we make one more transformation to the ''atomic basis'' $\{|\eta_i\rangle\}$, that diagonalizes the complex scaled atomic Hamiltonian

$$\langle\eta_i|H_{0,\theta}|\eta_j\rangle=E_i\delta_{ij}, \quad (20)$$

where

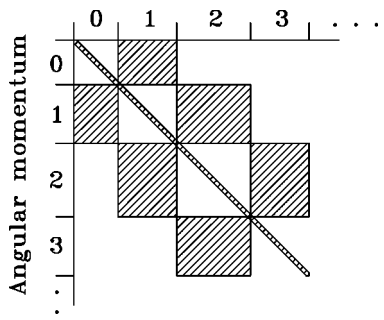

FIG. 1.The Hamiltonian matrix in the atomic basis.

$$H_{0,\theta}=-\frac{e^{-2i\theta}}{2}(\Delta_1+\Delta_2)-\frac{Ze^{-i\theta}}{r_1}-\frac{Ze^{-i\theta}}{r_2}+\frac{e^{-i\theta}}{r_{12}}. \quad (21)$$

In the dipole approximation the laser field only connects angular momenta differing by $|L-L'|=1$. The resulting structure of the overall Hamiltonian is depicted in Fig. 1.

At the laser intensities and frequencies in our calculations, the diagonal terms still make the dominant contribution to the time evolution. Therefore we time integrate in the ''interaction picture''

$$c(t)=a(t)+b(t), \quad (22)$$

$$i\frac{d}{dt}a(t)=\hat{H}_{0,\theta}a(t), \quad (23)$$

$$i\frac{d}{dt}b(t)=[\hat{H}_\theta(t)-\hat{H}_{0,\theta}]a(t)+\hat{H}_\theta(t)b(t). \quad (24)$$

Here $c(t)$ denotes the coefficient vector, and $\hat{H}_{0,\theta}$ and $\hat{H}_\theta$ are the operator matrices with respect to the $\{|\eta_i\rangle\}$ basis. For the decomposition of $c(t)$ into $a(t)+b(t)$, at the beginning of each time step we set

$$a(t_0)=c(t_0), \quad b(t_0)=0.$$

Since $\hat{H}_{0,\theta}$ is diagonal in our basis, the solution of Eq. (23) is trivial. Equation (24) is solved by a seven stage sixth-order explicit Runge-Kutta method (Butcher's method, given in Ref. [26]), which we found to be more CPU time efficient than lower-order methods. There were no problems with numerical stability, as we verified by comparing with lower-order methods at a few parameter points. The time step was automatically adapted by comparing every two integration steps with a single double-step size integration. The typical number of time steps was about 400 per optical cycle, which for our seven-stage method means about 3000 matrix-vector multiples per cycle. Computation times for the shorter pulses were about 1 hour on a 500-MHz DEC/Alpha work station.

III. RESULTS

A. Bound and doubly excited states

Before we discuss the results of the time propagation, we want to list the energies and widths of the most important bound and doubly excited states of He and H^- as obtained with the above basis. Table II compares the values of the first

TABLE II. Bound-state energies of He: (a) Calculated with the basis used for time propagation. (b) Literature values.

(a)	(b)	Ref.
$L=0$		
−2.903724377	−2.903724392	[27]
−2.14597404	−2.145974037	[27]
−2.06127198	−2.0612719	[27]
−2.0335877	−2.033586	[27]
$L=1$		
−2.123843088	−2.12384308	[27]
−2.05514636	−2.05514637	[27]
−2.0310696	−2.0310696	[19]
−2.0199059	−2.0199059	[19]
$L=2$		
−2.055620727	−2.05562071	[19]
−2.0312798	−2.0312798	[19]
−2.0200158	−2.0200158	[19]
−2.0138989	−2.0138981	[19]
$L=3$		
−2.0312551444	−2.03125514439	[20]
−2.0200029370	−2.02000293714	[20]
−2.0138906837	−2.01389068381	[20]
−2.010205246	−2.01020524808	[20]
(a)	(a)	
$L=4$	$L=6$	
−2.0200007108	−2.0102041204	
−2.0138893453	−2.0078125284	
−2.0102043836	−2.0061728509	
$L=5$	$L=7$	
−2.0138890346	−2.0078125124	
−2.0102041827	−2.0061728489	
−2.0078125737	−2.0049999968	

few bound-state energies of He that we obtained with the basis used in the time propagation, with reference values from literature. Several of our values are lower than the variational upper bounds from literature, but this does not indicate greater accuracy, since due to complex scaling our values are not upper bounds. Our accuracy is $\sim 10^{-8}$ a.u. for most energies given. The basis sizes are about 300 for each angular momentum. The functions are counted after removal of near-singular vectors from the basis (cf. Sec. II D), which is the number relevant for the time propagation. As an example, we listed in Table I above the basis set for $L=2$. It has been shown that literature values can be exactly reproduced with bases of size ~ 150 that are optimized for each state [19,20].

Table III gives lowest few doubly excited states of He from the time propagation. The states are labeled by the radial quantum numbers of the dominant single-electron contributions n_1 and n_2. Accuracies are of the order 10^{-4} a.u. for the energies and widths. At the very small widths the relative accuracies can become poor.

Finally, Table IV summarizes the bound and doubly excited state energies of H^-. We present the energies as they appear in the time propagation as well as values obtained in larger bases with state specifically adapted exponents α_s and β_s. Judging from the convergence behavior, we believe that our state-specific values are accurate to all except possibly the last digit quoted. One sees that some of them are more accurate than the literature values quoted. A special case is the shape resonance in $L=1$ just above the $H(n=2)$ threshold. It requires a minimum scaling angle of $\theta \approx 0.25$ to become manifest as an isolated eigenvalue of the scaled Hamiltonian. With the smaller angle used in the time propagation, the resonance state cannot be distinguished from the approximate continuous states that surround it.

TABLE III. Doubly excited states of He for $L=0-3$. (a) Values obtained with the basis used in the time propagation. (b) Literature values from references [29] ($L \leqslant 2$) and [28] ($L>2$).

(n_1,n_2)	(a)		(b)	
		$L=0$		
(2,2)	−0.777879	4.55×10^{-3}	−0.777868	4.53×10^{-3}
(2,2)	−0.621926	2.156×10^{-4}	−0.6219275	2.156×10^{-4}
(2,3)	−0.589892	1.37×10^{-3}	−0.589895	1.35×10^{-3}
(2,3)	−0.548085	6.8×10^{-5}	−0.5480855	7.8×10^{-5}
(3,3)	−0.353517	2.98×10^{-3}	−0.353537	3.004×10^{-3}
(3,3)	−0.317511	6.9×10^{-3}	−0.317455	6.67×10^{-3}
		$L=1$		
(2,2)	−0.6931347	1.366×10^{-3}	−0.6931349	1.3773×10^{-3}
(2,3)	−0.5970738	3.857×10^{-6}	−0.59707381	3.84399×10^{-6}
(2,3)	−0.5640865	2.93×10^{-4}	−0.56408514	3.01057×10^{-4}
(3,3)	−0.335611	6.92×10^{-3}	−0.3356269	7.023×10^{-3}
(3,3)	−0.2862	3.04×10^{-4}	−0.28595074	3.409×10^{-5}
(3,3)	−0.282855	1.63×10^{-3}	−0.28282897	1.46208×10^{-3}
		$L=2$		
(2,2)	−0.701938	2.360×10^{-3}	−0.7019457	2.3622×10^{-3}
(2,3)	−0.56925	6.9×10^{-4}	−0.569221	5.55×10^{-4}
(2,3)	−0.55640	3.6×10^{-4}	−0.5564303	2.01×10^{-5}
(3,3)	−0.34309	5.174×10^{-3}	−0.343173	5.155×10^{-3}
(3,3)	−0.31545	4.14×10^{-3}	−0.31553	4.305×10^{-3}
		$L=3$		
(2,3)	−0.5582830	1.297×10^{-5}	−0.55828	1.28×10^{-5}
(2,3)	−0.5322936	3.50×10^{-5}		
(3,3)	−0.3042474	3.24×10^{-3}	−0.30424	3.24×10^{-3}
(3,3)	−0.2780025	9.58×10^{-5}		

B. Excitation and ionization of He

Figure 2 shows the probability of excitation and ionization of He by $\cos^2$-shaped pulses of duration $T=157$ a.u. and peak intensity $I=0.004\,23$ a.u. $=2.97\times10^{14}$ W/cm^2. Note that in Ref. [8] the conversion to SI units was too small by a factor of 2. The frequencies cover the range from just above the five-photon ionization threshold to well above the single-photon ionization threshold. Below each of the thresholds one clearly distinguishes the enhancement of bound-state excitation due to resonances. The peaks below the one- and two-photon thresholds are due to resonances with the lowest P state (energy $=-2.123\,84$) and the lowest excited S state (energy $=-2.145\,97$), respectively. The resonances below the lower thresholds are not well separated due to the spectral width of the pulse. The pronounced dip in the bound-state excitation at $\omega=0.72$ is due to a Rabi-like oscillation.

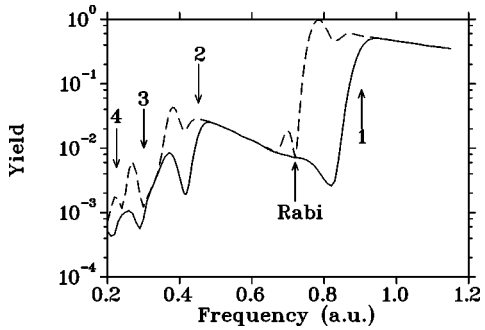

FIG. 2. Excitation and ionization of He by a $\cos^2$-shaped pulse of duration 3.8 fs and peak intensity 2.97×10^{14} W/cm^2 as a function of frequency. Solid line: ionization; dashed line: ionization plus bound state excitation. The arrows labelled by $n=1$, 2, 3, and 4 indicate n-photon ionization thresholds. The dip at frequency 0.72 is due to a Rabi oscillation.

When one increases the pulse duration, the minimum disappears completely, and reappears at a pulse duration of ~270. A third minimum appears at $T=380$ (Fig. 3). The oscillation period roughly corresponds to the Rabi period at the given parameters. The effect strongly depends on the pulse shape. Figure 4 compares excitation by $\cos^2$ pulses with excitation by Gaussian pulses. The pulse energy is 0.5 a.u. for both pulse shapes, and the widths of the vector potential envelopes were $T=157$ for the $\cos^2$ pulse and $T=92$ for the Gaussian pulse. With this choice the envelopes have the same width at $1/e$ of the maximum for both pulse shapes. One can see that the Rabi-like oscillations occur for both shapes, but they are more pronounced with the $\cos^2$ pulses.

One can also distinguish resonant enhancement of ionization, manifested by the coincidence of bound-state excitation peaks with ionization peaks. Most pronounced are the peaks at the three-photon resonance with the lowest P state at frequency $\omega=0.26$ and the two-photon resonance with the lowest excited S state at $\omega=0.38$; another resonance with the lowest D state is hidden in the slope to the two-photon ionization threshold. In spite of the massive bound state excitation at the single-photon resonance at $\omega=0.78$, weak coupling of the P state to the continuum leads only to a slight bump in the ionization rate at that frequency.

The lowest frequency of 0.2 in the figures is somewhat above the popular frequency of 0.1837 of a 248-nm wavelength laser. In Table V, we give the ionization yield at wave length 248 nm by a $\cos^2$ pulse of duration $T=40$ cycles $=32.8$ fs, which has a half-width of 20 optical cycles. The pulse parameters coincide with the ones used in Ref. [36] for the comparison with experiment. Our results are systematically lower by about 50% compared to Ref. [36]. We estimate that our results are converged to 10% accuracy or better (see below). Considering that we cover intensities all the way into the onset of saturation, the agreement is nevertheless satisfactory.

Recently another calculation for the same pulse was published [37]. Those values sizably oscillate around ours, and also around the results of Ref. [36]. The disagreement is particularly evident at the lower intensities, where convergence problems should be smaller. It appears, therefore, that calculations of Ref. [37] remain relatively far from convergence. A possible reason for the lack of convergence is the absence of doubly excited states from the basis of Ref. [37], although the velocity gauge used in that calculation always introduces at least virtual doubly excited states (cf. Sec. II B). The experimental number given in Ref. [36] is at least one order of magnitude smaller than all theoretical results and none of the calculations falls within the quite large upper error margin of the experiment.

Ionization is predominantly a single-electron effect, and all observations made above are qualitatively the same in a single-electron atom. Double excitation in turn is a genuine

TABLE IV. Bound and doubly excited states of H^- for $L=0$–3. (a) Values obtained with the basis used in the time propagation. (b) Values with a basis optimized for each state, and literature values. The values (b) are estimated to be converged to all digits given except for the last.

Energy	Width	Reference
	$L=0$	
-0.52775101689	0	present, (a)
-0.5277510165443	0	[30]
-0.1487764	1.7324×10^{-3}	present, (a)
-0.1487762	1.7332×10^{-3}	present, (b)
-0.1487765	1.731×10^{-3}	[31]
-0.12605	12×10^{-5}	present, (a)
-0.1260199	9.02×10^{-5}	present, (b)
-0.12601965	8.985×10^{-5}	[32]
-0.069006	1.4192×10^{-3}	present, (a)
-0.069006	1.4184×10^{-3}	present, (b)
-0.05615	23×10^{-5}	present, (a)
-0.0561434	8.8×10^{-5}	present, (b)
	$L=1$	
-0.12604986	1.36×10^{-6}	present, (a)
-0.12604986	1.36×10^{-6}	present, (b)
-0.1260495	1.165×10^{-6}	[32]
[a]		present, (a)
-0.1243856	7.0×10^{-4}	present, (b)
-0.12436	6.9×10^{-4}	[33]
-0.062708	1.17×10^{-3}	present, (a)
-0.062716	1.19×10^{-3}	present, (b)
-0.06871675	1.1914×10^{-3}	[34]
-0.058586	$<10^{-5}$	present, (a)
-0.0585718	8.988×10^{-6}	present, (b)
-0.05857181	8.986×10^{-6}	[34]
	$L=2$	
-0.127937	3.19×10^{-4}	present, (a)
-0.127937	3.12×10^{-4}	present, (b)
-0.12794175	3.1625×10^{-4}	[32]
-0.065954	1.654×10^{-3}	present, (a)
-0.0659531	1.6576×10^{-3}	present, (b)
-0.0659533	1.6581×10^{-3}	[35]
-0.056834	2.8×10^{-4}	present, (a)
-0.0568294	2.5302×10^{-4}	present, (b)
	$L=3$	
-0.056564	3.54×10^{-3}	present, (a)
-0.05655875	5.00×10^{-3}	present, (b)

[a]State cannot be distinguished from the surrounding continuum at the complex scaling angle of $\theta=0.22$ used in time propagation.

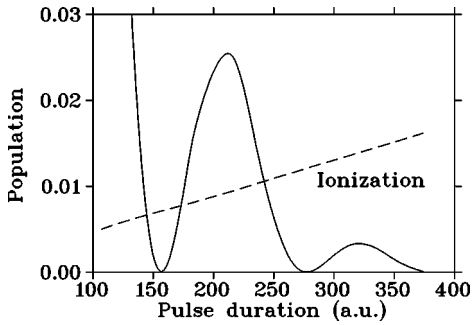

FIG. 3. Bound-state excitation as a function of pulse duration at frequency $\omega=0.72$. Solid line: total population of excited bound states. Dashed line: ionization. The distance between the minima is roughly the Rabi period.

two-electron effect. Figure 5 shows the population of the lowest doubly excited states with angular momentum $L=0$, 1, 2, and 3, after passage of a $\cos^2$-shaped pulse of duration $T=157$. The narrower peaks are due to multiphoton resonances between the ground and the respective doubly excited states with 2–6 photons. The population of the states with even L are enhanced in the range $\omega=0.6$–0.9. This enhancement is almost exactly proportional to the $^1P^0$ bound-state population, and the ratio between the populations was found to be proportional to the laser intensity. We therefore interpret it as a far off-resonant single-photon transition from the P to the S and D states brought about by the large bandwidth of the pulse. As with the Rabi oscillation of single excitation, the pulse shape is quite important, since with Gaussian pulses the phenomenon nearly disappears. Similarly, a longer pulse duration suppresses the effect.

C. Excitation and electron detachment from H^-

The binding energy of the only bound state of H^- is 0.027 75 a.u. Therefore, much lower laser intensities and frequencies lead to total electron detachment from H^-.

Figure 6 shows the photodetachment at a laser frequency of $\omega=0.03$ for intensities between 1×10^{11} and 8×10^{11} W/cm^2. At about 2×10^{11} W/cm^2 the single-photon ionization threshold rises above $\omega=0.03$ due to the ac Stark shift and roughly in the same intensity region two-photon ionization becomes dominant [5]. In our time-dependent calculations we can distinguish a bend in the detachment yield,

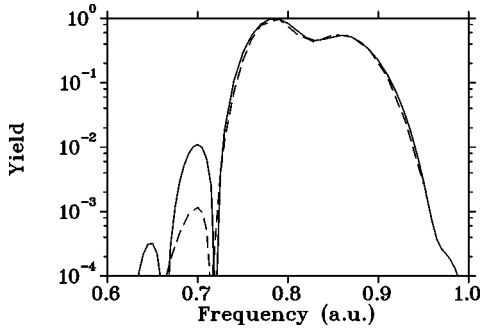

FIG. 4. Bound-state excitation for Gaussian and $\cos^2$ pulses as a function of frequency. The pulse energy is 0.5 a.u. for both shapes, and the pulse widths are $T=157$ for $\cos^2$ pulses (solid line) and $T=92$ for Gaussian pulses (dashed line).

TABLE V. Ionization yield for laser wavelength 248 nm and pulse duration $T=40$ optical cycles as a function of peak intensity I. The literature values are obtained by converting the generalized cross sections from Table 2 in Ref. [36] with the help of Eq. (16) in that reference.

I (W/cm^2)	Present	Ref. [36]
2×10^{14}	7.06×10^{-3}	8.13×10^{-3}
2.5×10^{14}	0.00105	0.00148
5×10^{14}	0.043	0.069
1×10^{15}	0.18	0.33

which moves toward the expected intensity of 2×10^{11} W/cm^2 with increasing pulse duration. The dashed lines are obtained by integrating the intensity-dependent detachment rates $\Gamma(I)$ from Ref. [5] with the pulse shapes used in our calculations. Saturation effects in the final detachment yield $Y(t=\infty)$ are included according to the equation

$$Y(t)=\int_{-\infty}^{t} dt'\ \Gamma[I(t')][1-Y(t')]. \tag{25}$$

As the instantaneous intensity, we defined

$$I(t):=[E_0 h(t)]^2/2, \quad E_0=\omega A_0. \tag{26}$$

This definition neglects terms with the time derivative of the envelope, whose contributions do not visibly change the

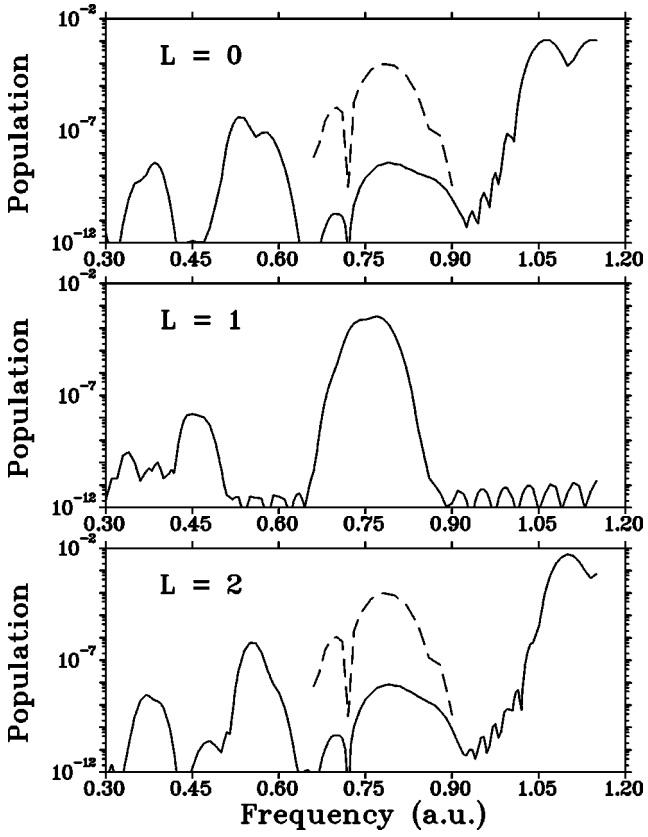

FIG. 5. Populations of the lowest doubly excited states with $L=0$, 1, and 2 after the passage of a pulse with $T=3.8$ fs with a peak intensity 2.97×10^{14} W/cm^2. Dashed lines: population of the lowest bound state with symmetry $^1P^0\times10^{-4}$.

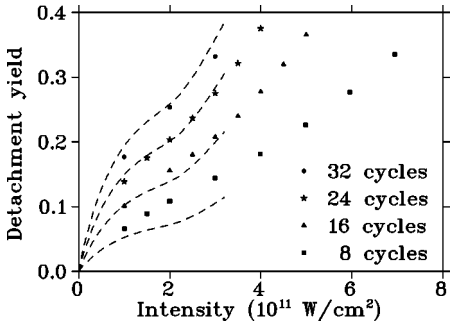

FIG. 6. Ionization of H^- by $\cos^2$-shaped pulses with laser frequency $\omega=0.03$ as a function of intensity for pulse durations $T=8$, 16, 24, and 32 optical cycles. The bend in the ionization yield is due to the closure of single-photon ionization channel by the ac Stark shift and the transition to two-photon ionization. Dashed lines: time-integrated Floquet rates from Ref. [5].

comparison. The agreement for the two longer pulses is quite good, except that the bend in the yield is somewhat more pronounced for the integrated rates. With the shorter pulses the integrated rate underestimates the true detachment. Also assuming the applicability of the rate concept at short pulses, the spectral width of the pulse could be sufficient to explain the higher yield: with a broad pulse the closure of the single-photon ionization channel is moved to higher intensities, thus effectively enhancing the yield. For a quantification of this hypothesis, rates $\Gamma(I)$ for frequencies other than $\omega=0.03$ would be required.

For the double excitation of H^-, one needs frequencies in the visible to low UV. Figure 7 shows the excitation of the relatively long-lived lowest autoionizing P state around the resonant frequency of $\omega=0.134$ and intensity 10^{13} W/cm^2. The resonance is shifted from its field-free position by about 0.001 for the ten-cycle pulses. Longer pulses of 20 cycles have a larger shift of ~ 0.002. In the limit of a constant laser field an ac Stark shift of the ground state by ~ 0.005 is expected by perturbatively extrapolating the data from Ref. [5].

D. Harmonic generation

With Eq. (6), we calculate the expectation value of the dipole $\vec{d}(t)$ as a function of time, from which we obtain the

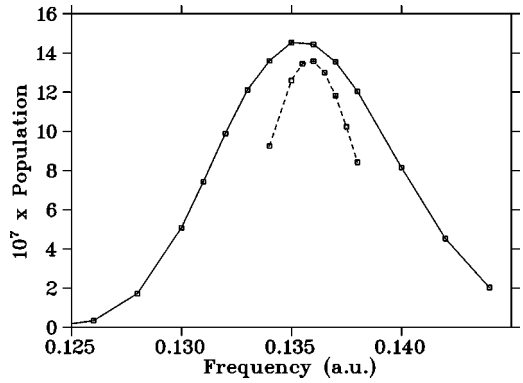

FIG. 7. Population of the lowest doubly excited P state of H^- by $\cos^2$-shaped pulses as a function of frequency. The peak intensity is 10^{13} W/cm^2, and the pulse durations $T=10$ optical cycles (solid line) and $T=20$ (dashed line).

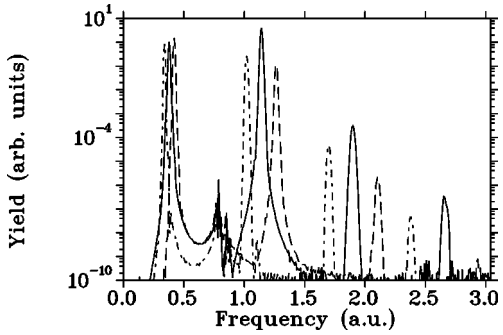

FIG. 8. Harmonic generation on H with a $\cos^2$ pulse of duration $T=40$ optical cycles and a peak intensity 2×10^{14} W/cm^2. The fundamental frequencies are 0.34 (dot-dashed line), 0.38 (solid line), and 0.42 a.u. (dashed line), respectively. The frequency 0.38 is two photon resonant, with the lowest excited S state. The structure around $\omega=0.8$ originates from bound-state excitations.

acceleration of the dipole by numerical differentiation. It would be more desirable to calculate the expectation values of the acceleration of the dipole $\ddot{\vec{d}}(t)$ directly, but unfortunately in the matrix elements of that operator integrals of form (18) with negative powers of r_1 or r_2 arise, which can only be calculated with considerable extra numerical effort (cf. Ref [25]).

The expectation values $\vec{d}(t)$ are sensitive to the wave function at larger distances. To obtain accurate results, we therefore added extra basis functions with smaller exponents to cover a longer range in r_1 and r_2. By this enlargement of the basis we were able to obtain satisfactory accuracies of $\lesssim 10\%$ up to the fifth harmonic for frequencies in the range 0.34–0.42 a.u. and intensity $I=2\times10^{14}$ W/cm^2. The frequencies include a strong resonance with the lowest excited S state that greatly enhances harmonic generation and leads to the dominance of the third harmonic over the first. Figure 8 summarizes the results obtained with a pulse duration of 40 optical cycles. Harmonics up to order 7 can be distinguished, and the resonant enhancement at $\omega=0.38$ is manifest. For reference we include Table VI with the peak heights.

E. Accuracy of the results

The limited expansion length for the wave function introduces the dominant error into our calculations. Now we study the effect of the truncations with respect to total angular momentum and radial basis functions.

Figure 9 compares the results of calculations with $L_{\max}=5$, 6, and 7 at peak intensity 2.97×10^{14} W/cm^2 and fre-

TABLE VI. Relative peak heights of harmonic generation by $\cos^2$ pulses of $T=40$ optical cycles, and peak intensity 2×10^{14} W/cm^2 for three different fundamental frequencies ω. The accuracies are 10% up to the fifth harmonic, and of the order 50% for the seventh harmonic.

	Harmonic order			
ω	1	3	5	7
0.34	0.85	0.25	4.8×10^{-5}	4.4×10^{-8}
0.38	1	3.9	3.2×10^{-4}	3.4×10^{-7}
0.42	1.46	0.11	2.1×10^{-6}	—

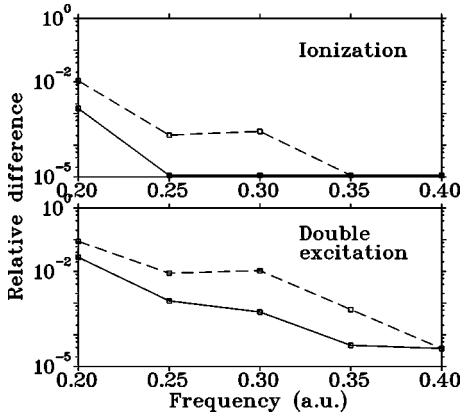

FIG. 9. Convergence of ionization and total double excitation with the maximum angular momentum $L_{\max}$. Dashed line: relative difference between calculations with $L_{\max}=5$ and 7; solid line: relative difference between $L_{\max}=6$ and 7. Intensity $=2.97\times10^{14}$ W/cm^2, pulse duration $T=157$.

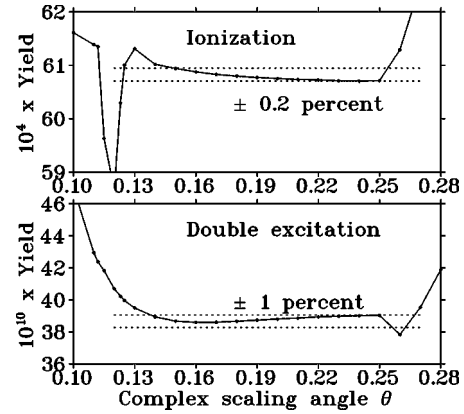

FIG. 10. Dependence of ionization and double excitation on the complex scaling angle θ. The dotted lines indicate estimated errors. The intensity is 2.97×10^{14} W/cm^2, the frequency is 0.4, and the pulse duration $T=157$.

quencies between 0.2 and 0.4. Only at the lowest frequencies is there a distinguishable effect on ionization with a relative difference between the calculations of $\lesssim1\%$. Double excitation is more sensitive to angular momentum truncation, since it is a much higher-order process, but still the relative error rises to only about 10%. Assuming exponential convergence, we can conclude that with $L_{\max}$ also for double excitation the error due to angular momentum truncation is $\lesssim1\%$ at the given parameters.

Convergence of the expansion in the internal coordinates r_1, r_2, and r_{12} is more difficult to investigate, since the basis rapidly grows when one increases the admissible powers of r_1, r_2, and r_{12}. Complex scaling provides an indirect estimate of the accuracy of the internal expansion. For an infinite basis, the results are independent of θ. Any dependence on θ must therefore be ascribed to the basis truncation. In practice, there is only a limited range of θ where the results vary little with θ. When θ is too small, the outgoing waves are only weakly damped, and one needs to describe a long oscillatory tail in the wave function, for which an L^2 expansion converges slowly. When, on the other hand, θ is too large, the complex scaled bound state wave functions have increasingly oscillatory character, which again is not well reproduced by the finite basis (cf. the Appendix). Figure 10 shows ionization and double excitation obtained with different scaling angles at laser frequency 0.39 a.u. One distinguishes a range of θ where the results are quite stable. The variation inside this range is of the same size as the variation when we increase the number of basis functions by a factor ~2, which supports our use of the variation with θ for an accuracy estimate. For the given parameters, the ionization varies less than 0.2%. The accuracies for double excitation are only slightly lower. At frequency $\omega=0.3$ the variation of ionization still remains within the 1% range, but double excitation varies by about 10%, which indicates that we approach the limits of numerically reliable results for multiphoton double excitation.

IV. SUMMARY AND CONCLUSIONS

The method introduced in this paper allows a numerical integration of the complete Schrödinger equation of a two-electron atom in a strong laser pulse with realistic frequency, intensity, and duration. This has been demonstrated on the systems of He and H^- with frequencies ranging from infrared to ultraviolet, intensities up to 10^{15} W/cm^2 and pulses as long as 160 fs.

The first important constituent of our method is an explicitly correlated basis set expansion, which allows us to reproduce the atomic structure to essentially any desired accuracy at moderate expansion length. This includes positions and widths of doubly excited states, where we obtain accuracies that rival and in some cases exceed literature values.

The second ingredient of our method, complex scaling, was formally introduced as a method of imposing strictly outgoing boundary conditions. We cannot at present give a mathematically rigorous theory for the use of complex scaling in a time-dependent calculation, but we provide heuristic arguments and numerical evidence that it indeed is equivalent to the regular Schrödinger equation with strictly outgoing boundary conditions. The technical advantage of complex scaling is that the expansion length remains short.

Convergence was investigated for the whole range of parameters, and indicates accuracies between fractions of a percent at higher laser frequencies and at least 10% for the majority of the data. Only at the seventh harmonic peak in our example, and for double excitation at lowest laser frequencies, do accuracies remain unsatisfactory.

The numerically most challenging combination of parameters was used for He exposed to pulses of duration ~32 fs at the wave length of 248 nm and peak intensities up to 10^{15} W/cm^2, where we reach an accuracy of the ionization yield of about 10%. A previous calculation for the same pulses [36] agreed qualitatively with ours, but exceeded our result by about 50% at the highest intensity. A more recent calculation [37] deviated more strongly also at the lower intensities.

Another comparison with existing theoretical work could be performed with a Floquet calculation for the electron detachment from H^-. Quite satisfactory agreement was found for pulses of at least 16 optical cycles. Shorter pulses may not be expected to compare well with a Floquet calculation for constant intensity.

We believe that our results should serve as a benchmark

for future calculations of two-electron systems. This refers to both complete two-electron calculations as well as model calculations. It may be expected that for harmonic generation and ionization a single-electron description will be found to be satisfactory in a range of parameters.

If necessary, our method allows extensions in several directions. To extend the range of accessible parameters is predominantly a question of more computer power, although technical modifications in the calculation of the matrix elements are also required to control the loss of accuracy. A second obvious extension is the introduction of an electronic core to model effective two-electron atoms like Mg. Finally, the interpretation of the complex scaled wave function adopted in this paper, which takes the back-scaled wave function as an approximation to the regular solution with outgoing-wave boundary conditions, suggests that electron spectra can be determined. Whether this is numerically feasible and practical remains to be investigated.

ACKNOWLEDGMENTS

We wish to thank Robin Shakeshaft and Marcel Pont for numerous fruitful discussions. A.S. acknowledges support from the APART program of the Austrian Academy of Sciences and is thankful for the hospitality he enjoyed during several stays at the Université Catholique de Louvain. B. P. is chercheur qualifié au Fonds National de la Recherche Scientifique of Belgium.

APPENDIX

Here we deduce the relation between outgoing-wave boundary conditions and complex scaling. We first assume that one can write the radial wave function in the form

$$\Psi(r;t)=\int_{-\infty}^{\infty} dk\; c(k,t)\Phi_k(r), \tag{A1}$$

where Φ_k have the asymptotic behavior $\sim e^{ikr}$, and Ψ solves the Schrödinger equation

$$i\frac{d}{dt}\Psi(r;t)=H(r;t)\Psi(r;t). \tag{A2}$$

For the sake of brevity we have omitted the part of the expansion with square-integrable functions. [For the Coulomb potential the asymptotic behavior is more precisely $\sim\exp(ikr-i\,\ln 2|k|r/k)$.] In terms of the expansion coefficients $c(k;t)$, Eq. (A2) can be written as

$$i\frac{d}{dt}c(k;t)=\int_{-\infty}^{\infty} dk' h(k,k';t)c(k';t). \tag{A3}$$

Outgoing boundary conditions mean that one solves Eq. (A3) restricted to $k>0$:

$$i\frac{d}{dt}c^{+}(k;t)=\int_{0}^{\infty} dk' h(k,k';t)c^{+}(k';t). \tag{A4}$$

The time-dependent wave function with outgoing boundary conditions is then

$$\Psi^{+}(r;t):=\int_{0}^{\infty} dk' c^{+}(k';t)\Phi_{k'}(r). \tag{A5}$$

In order to relate $\Psi(r,t)$ to the complex scaled wave function, we must assume that $\Psi(r,t)$ and its time derivative $d\Psi(r,t)/dt$ are analytic functions of r for any analytic initial state $\Psi(r,t=0)$. This assumption is nontrivial: for example, it is known to be valid for the Hamiltonian of the field-free hydrogen atom, while it is obviously violated for potentials that are nondifferentiable at any point other than $r=0$. Under this assumption, the analytically continued wave function $\Psi(\eta r;t)$, $\mathrm{Im}(\eta)>0$ solves the ''complex scaled'' Schrödinger equation

$$i\frac{d}{dt}\Psi(\eta r;t)=H(\eta r;t)\Psi(\eta r;t), \tag{A6}$$

which is the analog of Eq. (5) for a single radial coordinate. If we further assume that the expansion functions Φ_k are analytic, the expansion coefficients c_η

$$\Psi(\eta r;t)=\int_{-\infty}^{\infty} dk\; c_\eta(k,t)\Phi_k(\eta r), \tag{A7}$$

do not depend on η:

$$c_\eta(k,t)\equiv c(k,t). \tag{A8}$$

From this it follows that the kernel of the time integration $h(k,k';t)$ also does not depend on η. We see that the two equations (A2) and (A6) describe exactly the same dynamics. The important difference is that due to the asymptotic behavior of the expansion functions $\Phi_k(\eta r)\sim\exp(ik\eta r)$ in Eq. (A6), we can distinguish $k>0$ from $k<0$ by their norms: ''ingoing waves'' $k<0$ grow exponentially, while ''outgoing waves'' $k>0$ become square integrable. Because of the exponential divergence, any function

$$\int dk\; a(k)\Phi_k(\eta r) \tag{A9}$$

will diverge, if $\int_{-\infty}^{0} dk|a(k)|^2>0$. Consequently, if $\Psi(\eta r;t)$ contains ingoing waves, it will not be square integrable. To obtain a solution with outgoing waves only, we solve the differential equation (A6) restricted to the space of square integrable functions $\|\Psi^{+}(\eta r;t)\|<\infty$. Since $h(k,k';t)$ does not depend on η, the coefficients of the expansion

$$\Psi^{+}(\eta r;t)=\int_{0}^{\infty} dk' c^{+}(k';t)\Phi_{k'}(\eta r) \tag{A10}$$

are the same as in Eq. (A5), and the outgoing-wave solution is obtained by substituting ηr with r.

As an initial condition for Eq. (A6), we use a field-free bound state. For the class of ''dilation analytic'' [13] potentials, which include the Coulomb potential, the bound-state functions are known to be analytic functions of r. This is trivial to verify for the complex scaled Hamiltonian of the two-body Coulomb problem,

$$\left(-\frac{1}{2\eta^2}\Delta - \frac{Z}{\eta r} \right) \Phi_i(\eta r) = E_i \Phi_i(\eta r), \qquad \text{(A11)}$$

where $\Phi_i(r)$ is a hydrogenic bound-state function. For computation it is useful to keep in mind that, for example, the radial ground-state eigenfunction $\eta r \exp(-\eta r)$ becomes increasingly oscillatory with increasing $\mathrm{Im}(\eta)$, which is opposite to the outgoing waves, where larger $\mathrm{Im}(\eta)$ causes a stronger damping. Oscillatory functions are generally more difficult to represent numerically, and the choice of $\eta = e^{i\theta}$ will depend on whether the outgoing-wave or the bound-state parts of Ψ_η are more important.

[1] P. G. Burke, P. Francken, and C. J. Joachain, Europhys. Lett. **13**, 617 (1990); J. Phys. B **24**, 761 (1991).
[2] P G. Burke and V. M. Burke, J. Phys. B **30**, L383 (1997).
[3] J. Parker, K. T. Taylor, C. W. Clark, and S. Blodgett-Ford, J. Phys. B **29**, L33 (1996).
[4] J. Zhang and P. Lambropoulos, J. Phys. B **28**, L101 (1995).
[5] J. Purvis *et al.*, Phys. Rev. Lett. **71**, 3943 (1993).
[6] R. Gebarowski *et al.*, J. Phys. B **30**, 2505 (1997).
[7] J. Zhang and P. Lambropoulos, Phys. Rev. Lett. **77**, 2186 (1996).
[8] A. Scrinzi and B. Piraux, Phys. Rev. A **56**, R13 (1997).
[9] W. Reinhardt, Annu. Rev. Phys. Chem. **33**, 223 (1978).
[10] E. Cormier and P. Lambropoulos, J. Phys. B **29**, 1667 (1996).
[11] K. Kulander, Phys. Rev. A **35**, 445 (1987).
[12] J. Zhang (unpublished).
[13] M. Reed and B. Simon, *Methods of Modern Mathematical Physics* (Academic, New York, 1982), Vol. 4, p. 183 ff.
[14] M. Pont, D. Proulx, and R. Shakeshaft, Phys. Rev. A **44**, 4486 (1991).
[15] E. Huens and B. Piraux, Phys. Rev. A **47**, 1568 (1993).
[16] A. Buchleitner, D. Delande, and J.-C. Gay, J. Opt. Soc. Am. B **12**, 505 (1995).
[17] S. D. Parker and C. W. McCurdy, Chem. Phys. Lett. **156**, 483 (1989).
[18] H. F. King, J. Chem. Phys. **46**, 705 (1967).
[19] A. Kono and Sh. Hattori, Phys. Rev. A **29**, 2981 (1994).
[20] J. S. Sims and W. C. Martin, Phys. Rev. A **37**, 2259 (1988).
[21] E. P. Wigner, in *Quantum Theory of Angular Momentum*, edited by L. C. Biedenharn and H. van Dam (Academic, London, 1965), p. 87.
[22] D. A. Varshalovich, A. M. Moskalev, and V. K. Khersonskij, *Quantum Theory of Angular Momentum* (World Scientific, Singapore, 1989).
[23] A. Scrinzi, J. Phys. B **29**, 6055 (1996).
[24] A. Bürgers, D. Wintgen, and J.-M. Rost, J. Phys. B **28**, 3163 (1995).
[25] A. Scrinzi, Phys. Rev. A **45**, 7787 (1992).
[26] L. Lapidus and J. H. Seinfeld, *Numerical Solution of Ordinary Differential Equations* (Academic, New York, 1973).
[27] C. L. Pekeris, Phys. Rev. **126**, 1470 (1962): Y. Accad, C. L. Pekeris, and B. Schiff, Phys. Rev. A **4**, 516 (1971).
[28] E. Lindroth, Phys. Rev. A **49**, 4473 (1994).
[29] Y. K. Ho, Phys. Rev. A **34**, 4402 (1986); Z. Phys. D **21**, 191 (1991); Y. K. Ho and A. Bhatia, Phys. Rev. A **44**, 2895 (1991).
[30] G. W. F. Drake, Nucl. Instrum. Methods Phys. Res. B **31**, 7 (1988).
[31] Y. K. Ho, Phys. Rev. A **23**, 2137 (1981).
[32] Y. K. Ho, Phys. Rev. A **52**, 375 (1995).
[33] Y. K. Ho and A. Bhatia, Phys. Rev. A **48**, 3720 (1993).
[34] Y. K. Ho, Phys. Rev. A **45**, 148 (1992).
[35] A. Bhatia and Y. K. Ho, Phys. Rev. A **41**, 504 (1990).
[36] D. Charalambidis *et al.*, J. Phys. B **30**, 1467 (1997).
[37] Th. Mercouris, S. Dionissopoulou, and C. A. Nicolaides, J. Phys. B **30**, 4751 (1997).